Received: 20 October 2022 | Revised: 21 December 2022 | Accepted: 8 January 2023

DOI: 10.1111/ffe.13951

SPECIAL ISSUE ARTICLE

FFEMS Fatigue & Fracture of Engineering Materials & Structures WILEY

Crack-tip blunting and its implications on fracture of soft materials

Andrea Spagnoli[1] | Roberto Brighenti[1] | Matteo Montanari[1] | Michele Terzano[2]

[1]Department of Engineering and Architecture, University of Parma, Parma, Italy

[2]Institute of Biomechanics, Graz University of Technology, Graz, Austria

Correspondence
Andrea Spagnoli, Department of Engineering and Architecture, University of Parma, Parco Area delle Scienze 181/A, 43124 Parma, Italy.
Email: spagnoli@unipr.it

Funding information
EU Horizon 2020 Research and Innovation Programme (H2020-WIDESPREAD-2018, SIRAMM), Grant/Award Number: 857124

Abstract

Fracture of compliant materials is preceded by large deformations that reshape initially sharp cracks into rounded defects. This phenomenon, known as elastic crack blunting, is peculiar of rubber-like polymers and soft biological tissues, such as skin, vessel walls, and tendons. With this work, we aim to provide a discussion on crack-tip blunting and its implications in terms of tearing resistance and flaw tolerance of soft elastic materials. The characteristic features of the crack-tip zone in the framework of nonlinear elasticity are reviewed analytically and with the help of finite element analyses on pure shear cracked geometries. Specifically, the strain-hardening behavior typical of soft biological tissues is addressed, and we illustrate its effect on crack-tip blunting, in terms of a local radius of curvature at the crack tip. A simplified geometrically nonlinear model, proposed to describe the progressive blunting at the crack tip and its effect on flaw tolerance, is validated through finite element analyses and experimental tests on silicone samples. We show how this can lead to a simplified criterion to define the fracture condition in nonlinear soft materials.

KEYWORDS

biomaterials, blunting line, crack tip displacement, hyperelastic material

1 | INTRODUCTION

Soft materials represent a large class of natural and engineered compounds, such as polymers, gels, foams, colloids, and the majority of the tissues in living beings.[1] Although their microstructure can be quite diverse, they share the common feature of being highly compliant when subjected to mechanical or thermal stimuli. This unique capability has various important implications, which explains the large research interest in the fields of solid mechanics, material science and bioengineering toward soft materials.[2,3] In this work, we focus on the implications of the compliance of soft materials in terms of the fracture process. Taking advantage of the similarity in the elastic behavior between biological tissues and soft polymers,[4] we aim to explore concepts and applications of actual relevance in the biomedical field, such as cutting and puncturing of soft tissues during surgery.[5,6]

Fracture mechanics of soft materials are drastically different from traditional engineered materials, such as glass or metals, and contradict the grounding assumptions of linear elastic fracture mechanics (LEFM). When considering the region around the tip of a crack in a soft material, large deformations become relevant on scales comparable to the characteristic macroscale geometry.[2,7] This prevents the approximation to the linearized theory of elasticity on which LEFM is grounded. As a consequence, the description of the crack-tip displacement and stress fields follows a drastically different mathematical treatment, as systematically analyzed in the pioneering research of Knowles and Sternberg.[8] At the same time, the energy-based description of fracture retains its validity for any material where dissipation is confined to a negligible process zone. Along this line, Rivlin and co-workers[9,10] established the framework on which theoretical and experimental fracture mechanics of soft materials is still based today.

The peculiarity of the crack-tip region in soft materials has been comprehensively reviewed by Long et al,[11] while a recent review of fracture in soft elastic materials can be found in the authors' work.[12] The asymptotic stress field is drastically different from that of LEFM and is strongly affected by strain hardening. Strain hardening is observed in certain class of rubbers and becomes particularly relevant in collagenous soft tissues.[13] It has important influences in the stress distribution around the tip of a crack and has been found to influence the mechanism of crack propagation.[11] Another distinctive aspect of the fracture process of soft materials is the transition from a sharp crack to a blunted notch before propagation, a phenomenon that goes under the name of elastic crack blunting.[14] Blunting mitigates the effect of stress concentrations caused by cracks and can be correlated to the remarkable property of flaw tolerance. This is defined as the insensitivity of a material to cracks and defects and has been recently investigated experimentally and numerically.[3,15]

In the present work, we briefly summarize the analytical crack-tip fields in nonlinear elastic materials, focusing in particular on a class of isotropic exponential strain-hardening models commonly applied to elastomers and biological tissues. Through refined finite element (FE) analyses at the crack tip, we obtain the deformed profiles of the crack under mode I loading and compute a local radius of curvature at the crack tip, which provides a measure of the elastic blunting of the crack under loading. In order to investigate the implications of this blunting on crack propagation and flaw tolerance, we apply a recently proposed geometrically nonlinear model[12] and compare its predictions to experiments on silicone specimens containing cracks. The final discussion attempts to highlight the relevance of nonlinearity and blunting in order to understand fracture of soft tissues.

2 | CRACK-TIP FIELDS IN NONLINEAR ELASTICITY

In this section, we review the basics of the analytical formulation and present some results from FE analyses of the crack-tip fields in nonlinear elasticity. The reader is referred to Long et al[11] and references therein for a more complete overview. The theoretical background concerning finite strain continuum mechanics and hyperelasticity of soft tissues is also briefly summarized.

2.1 | Strain hardening hyperelasticity in isotropic incompressible solids

Rubber-like materials and soft biological tissues are characterized by large deformations, ruling out the application of the linearized theory of elasticity on which LEFM is based. Deformation can be described by the nonlinear mapping χ, such that $\boldsymbol{x}=\chi(\boldsymbol{X})$, where $\boldsymbol{X}$ and $\boldsymbol{x}$ denote the position of a material point in the initial (reference) and deformed (current) configurations. Accordingly, the deformation gradient $\mathbf{F}(\boldsymbol{X})$ is a two-point tensor defined as $\mathbf{F}(\boldsymbol{X})=\partial\chi(\boldsymbol{X})/\partial\boldsymbol{X}$.[16] Various definitions of strain exist in nonlinear mechanics. Here, we adopt the symmetric left Cauchy–Green strain tensor $\mathbf{b}=\mathbf{F}\cdot\mathbf{F}^{\mathrm{T}}$, which represents the deformation measure in the current configuration. Let us now consider an isotropic hyperelastic material and postulate the existence of a strain-energy function expressed in terms of the principal invariants of $\mathbf{b}$

$$I_1=\mathbf{b}:\mathbf{I},\ I_2=J^2\mathbf{b}^{-1}:\mathbf{I},\ I_3=\det\mathbf{b}, \tag{1}$$

where $J=\det\mathbf{F}$ is the volume ratio and $\mathbf{I}$ is the second-order identity tensor. Introducing the assumption of material incompressibility, which applies with good approximation to rubber-like and biological materials, the strain-energy function is written as

$$\Psi=\hat{\Psi}[I_1(\mathbf{b}),I_2(\mathbf{b})]-p(J-1), \tag{2}$$

where p serves as Lagrange multiplier to enforce incompressibility.

In the following, we focus on a strain-energy function, which depends on the first strain invariant only and can be employed to model the effect of strain hardening, that is, the nonlinear increase of stress with deformation observed in biological tissues.[17] The expression, known as generalized neo-Hookean (GNH) model, is given by[8]

$$\hat{\Psi}[I_1(\mathbf{b});\mu,b,n]=\frac{\mu}{2b}\left\{\left[1+\frac{b}{n}(I_1-3)\right]^n-1\right\}, \qquad (3)$$

where μ is the initial shear modulus and b,n are material parameters. Note that $n>0$ is the parameter controlling strain hardening, with $n=1$ corresponding to the well-known neo-Hookean formulation.

A standard procedure leads to the fundamental constitutive equation of isotropic nonlinear elasticity directly expressed in terms of the left Cauchy-Green strain tensor, such that the Cauchy stress tensor is[16]

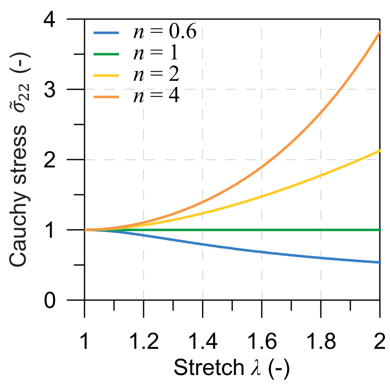

FIGURE 1 Dimensionless Cauchy stress $\tilde{\sigma}_{22}$ against stretch λ in the GNH model, with $b=1$ and $n=0.6-4$ for a pure-shear planar deformation. 1-col figure [Colour figure can be viewed at wileyonlinelibrary.com]

$$\boldsymbol{\sigma}=2\mathbf{b}\cdot\frac{\partial\hat{\Psi}}{\partial\mathbf{b}}-p\mathbf{I}=J^{-1}\psi_1\mathbf{b}-p\mathbf{I}, \qquad (4)$$

where the stress coefficient for the GNH model is $\psi_1=2\partial\hat{\Psi}(I_1)/\partial I_1=\mu\left[1+\frac{b}{n}(I_1-3)\right]^{(n-1)}$.

To illustrate the stress–strain curve of the GNH model, a pure shear deformation is considered, which is defined by the following deformation gradient

$$\mathbf{F}=\boldsymbol{e}_1\otimes\boldsymbol{E}_1+\lambda\boldsymbol{e}_2\otimes\boldsymbol{E}_2+\lambda^{-1}\boldsymbol{e}_3\otimes\boldsymbol{E}_3, \qquad (5)$$

where $\boldsymbol{e}_i,\boldsymbol{E}_I$, with $i,I=1,2,3$, represent the unit vectors of the current and reference Cartesian bases. The dimensionless reduced Cauchy stress $\tilde{\sigma}_{22}=\sigma_{22}/\mu(\lambda^2-\lambda^{-2})$, obtained analytically for a plane stress case ($\sigma_{33}=0$), is shown in Figure 1 as a function of the stretch λ.

2.2 | Analytical crack-tip fields in plane stress

We briefly review here the analytical solutions for the crack-tip fields in a two-dimensional plane stress problem for a GNH material, originally derived by Geubelle and Knauss[18] and more recently elaborated by Long et al.[19]

Let us start by considering a a thin sheet of hyperelastic material containing a crack. A local reference system X_1,X_2 is centered at the tip, so that the crack faces are coincident with the line $X_1<0,X_2=0$ in the initial configuration (Figure 2A). Upon loading, the crack faces

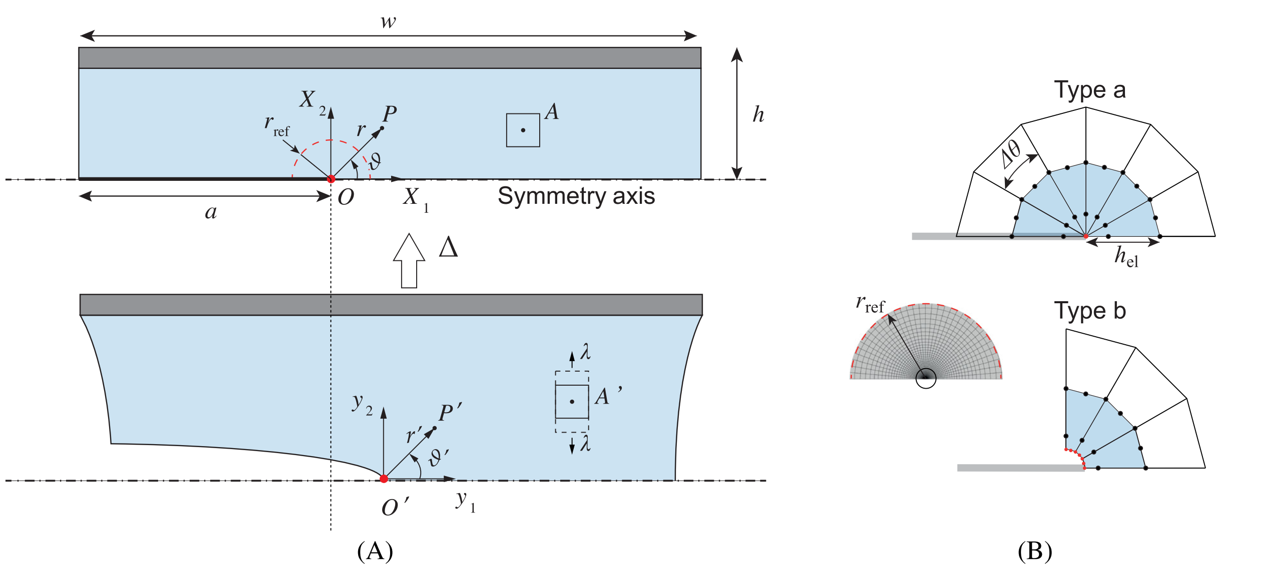

FIGURE 2 (A) Sketch of the pure-shear geometry adopted in FE analyses of the crack-tip fields in the reference and current configurations, with local axes centered at the crack tip. (B) Detail of the FE mesh defined in the crack-tip region, used to infer the stress singularities (type a) and for the crack-tip blunting (type b). 2-col figure [Colour figure can be viewed at wileyonlinelibrary.com]

open up and points in the deformed configuration can be referred to the current coordinates of the translated crack tip, defined as

$$y_i(\boldsymbol{X}) = x_i(\boldsymbol{X}) - x_i(\boldsymbol{X}=\boldsymbol{0}), \quad i=1,2, \tag{6}$$

where $\boldsymbol{X}=\boldsymbol{0}$ indicates the coordinates of the crack tip in the reference configuration. The hypothesis of a symmetric opening crack (Mode I) is expressed by $y_1(X_1,X_2)=y_1(X_1,-X_2)$ and $y_2(X_1,X_2)=-y_2(X_1,-X_2)$. We also introduce a planar cylindrical reference system r,ϑ, with $r=\sqrt{X_iX_i}$ and $\vartheta=\tan^{-1}(X_2/X_1)$. The crack-tip displacement field can be written in a separable form for $r\to 0$ as

$$y_i = r^{p_i} g_i(\vartheta,n) + o(r^{p_i}),\ i=1,2,\ -\pi\le\vartheta\le\pi, \tag{7}$$

where the symbol o is here used to denote higher order terms in the asymptotic expansion. In (7), p_i represents the order of the crack-tip singularity, with the condition $p_1>p_2$. The angular functions $g_i(\vartheta,n)$ must respect symmetry: Specifically, $g_1(\vartheta,n)$ is an even function, implying that $g_1(\vartheta=\pi,n)=g_1(\vartheta=-\pi,n)$; $g_2(\vartheta,n)$ is an odd function, with $g_2(\vartheta=0,n)=0$ and $g_2(\vartheta=\pi,n)=-g_2(\vartheta=-\pi,n)$. Furthermore, the parameter n must satisfy the requirement $n>0.5$ to ensure the ellipticity of the equilibrium equations of the elastic problem. The complete expressions of the crack-tip displacements are[19]

$$y_1 = \begin{cases} C_1 r^d g_1(\vartheta,n) & \text{if } n<1.46 \\ C_1 r^{(1+1/4n)} \tilde{g}_1(\vartheta,n) & \text{if } n>1.46 \end{cases}, \tag{8a}$$

$$y_2 = C_2 r^{(1-1/2n)} g_2(\vartheta,n), \tag{8b}$$

where $C_1,C_2>0$ are amplitudes that depend on the specimen geometry and loading conditions, while the expression of the exponent $d<1+1/4n$ was computed by Geubelle and Knauss.[18] The angular even functions in Equation (8a), $g_1(\vartheta,n)$ and $\tilde{g}_1(\vartheta,n)$, are different depending on whether the material parameter n is less or greater than 1.46, respectively.

Turning our attention to the crack-tip stress field, the normal and parallel Cauchy stress components are characterized by the following asymptotic expressions with respect to the cylindrical reference coordinates

$$\sigma_{22} = \mu \frac{b^{n-1}}{n^n}\left(\frac{2n-1}{2n}\right)^{2n} C_2^{2n} f_{22}(\vartheta,n) r^{-1}, \tag{9a}$$

$$\sigma_{11} = \begin{cases} \mathcal{O}\left(r^{2d-3+1/n}\right) & \text{if } n<1.46 \\ \mathcal{O}\left(r^{-1+3/2n}\right) & \text{if } n>1.46 \end{cases}, \tag{9b}$$

where the Landau symbol $\mathcal{O}$ identifies the asymptotic behavior of the stress component and $f_{22}(\vartheta,n)$ is an even angular function[19] Equation (9) shows that the asymptotic normal Cauchy stress σ_{22} is controlled by a single amplitude parameter C_2. As pointed out by Long et al,[19] this can be determined from a closed-form expression by computing the path-independent J-integral.

2.3 | FE analyses of the crack-tip region

We have employed FE analyses to obtain a complete map of the deformation and stress fields in the crack-tip region. A pure-shear geometry, often adopted in fracture testing of rubber-like materials,[9] was considered, consisting of a long thin strip of height $2h$ and width $w=10h$, with an edge crack $a=2.5h$ (Figure 2A). A uniform displacement Δ is imposed in the direction parallel to the short edges, such that $\lambda=1+\Delta/h$ defines the applied stretch. The specimen thickness is negligible with respect to other dimensions so that a state of plane stress is assumed. Due to symmetry, only half geometry can be modeled and pertinent constraints were added to the lower edge of the specimen. Mesh design is particularly critical in order to capture the asymptotic behavior of the crack-tip fields.[20] We have used eight-node plane stress elements to mesh the far-field domain, and a refined fan-shaped mesh zone of radius $r_{\text{ref}}=0.1h$, centered at the crack tip (Figure 2B). The solution accuracy is ensured by a proper choice of the characteristic element size h_{el} and of the angular span $\Delta\theta$. In this work, the smallest element size was taken equal to $h_{\text{el}}=10^{-5}h$ and the angular span was $\Delta\theta=5^\circ$. The model was solved using the implicit static solver of the commercial FE software Abaqus. The GNH model (3) was implemented through a user-defined material subroutine.

The crack-tip displacement field obtained from the FE analyses is illustrated in Figure 3A. The crack flank profile is obtained from the deformed coordinates of points located at $\vartheta=\pi$ within the region of reference radius r_{ref}, for a pure-shear stretch $\lambda=1.5$. The results show a remarkable influence of the strain hardening parameter n. In particular, the GNH model for $n\to 0.5$ displays an enhanced phenomenon of crack-tip blunting that progressively mitigates at higher values of the parameter n.[18] Figure 3B quantifies the crack-tip blunting through the variation of a local curvature as a function of the stretch. The radius of curvature ϱ was computed numerically from the deformed coordinates y_1,y_2 for $\vartheta=\pi$ as the radius of the best fitting circle within a distance equal to $10^{-3}h$ from the crack-tip. To further appreciate the effect of strain hardening on the local curvature, the ratios between the crack-tip radius at $\lambda=1.5$ and that at

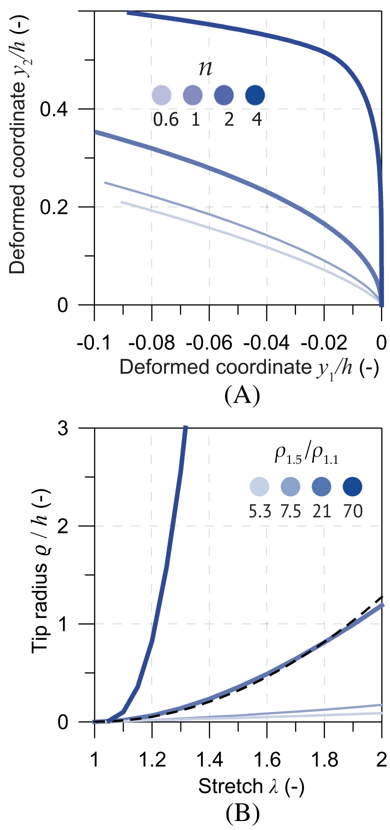

FIGURE 3 (A) Crack-tip displacement field from FE analyses, for $\vartheta = \pi$ and $\lambda = 1.5$. (B) Crack-tip radius in a region $r/h = 10^{-3}$ as a function of the stretch λ. The inset shows the ratios between the crack-tip radius at $\lambda = 1.5$ and that at $\lambda = 1.1$. Also shown is the LEFM solution (10) (dashed line). 1-col figure [Colour figure can be viewed at wileyonlinelibrary.com]

$\lambda = 1.1$ was computed. An increase by almost 70 times for $n = 0.6$, in contrast to a fivefold rise when $n = 4$, can be observed. As a comparison, the solution for LEFM is also added to Figure 3. Accordingly, the crack-tip radius evolves with the stretch as

$$\varrho = \frac{4}{\pi} h (\lambda - 1)^2, \tag{10}$$

which is derived from the expression of an elliptical crack flank, $\varrho = (4/\pi)(K/E)^2$ with $K = \sqrt{GE} = E(\lambda - 1)\sqrt{h}$ being the energy release rate $G = Eh(\lambda - 1)^2$, for the pure-shear configuration under consideration.[21]

The normalized Cauchy stress components σ_{11}/μ and σ_{22}/μ obtained from FE analyses are illustrated in Figure 4, corresponding to $\vartheta = 0$ and a pure-shear stretch $\lambda = 1.5$. The stress values were extracted from integration points of elements ahead of the crack tip enclosed in the circular region of reference radius r_{ref}, extrapolated to the nodes and plotted on a double logarithmic plot as a function of the reference distance r/h. The order of the singularity predicted by (9) is represented in each plot by lines that were fitted to the numerical points.

3 | MODEL OF CRACK-TIP BLUNTING

A model to describe the crack-tip blunting was recently proposed by the authors.[12] Below, we briefly summarize this approach and compare its predictions with experiments and FE analyses.

3.1 | Analytical formulation

Within the framework of LEFM, we can consider crack-tip blunting in terms of the reshaping of an initially sharp crack in a linear elastic material. In particular, if we assume that the crack evolves into an elliptical shape after deformation, we can predict the local stress from the pioneering works of Inglis on elliptical cracks.[22] At this point, we anticipate that, although developed for a linear elastic material, the model proposed includes geometric nonlinearity through an incremental update of the deformed crack profile.

Let us consider an ellipse whose major and minor semi-axes are denoted by a and b (Figure 5). The local stress and displacements can be computed from the general solution of an elliptical hole in an infinite elastic plate.[23] Adopting curvilinear elliptical coordinates (ξ, η), the semiaxes are equal to $a = c\cosh\xi_0$ and $b = c\sinh\xi_0$, where $c = \sqrt{a^2 - b^2}$ is the focal distance and $\xi = \xi_0 = \text{acosh}(a/c)$ is the equation of the ellipse boundary. These expressions hold for an ellipse with $a > b$, otherwise a and b need to be exchanged. The complete solution is available in the literature.[24]

We now consider the ellipse in an infinite plate loaded remotely by a uniform stress σ. Loading is applied in increments $\mathrm{d}\sigma^i$ and stress and displacements are computed in the points of intersection with the reference axes (X_1, X_2), denoted as $P_{\max} = P(X_1 = a, X_2 = 0) = P(\xi_0, 0)$ and $P_{\min} = P(X_1 = 0, X_2 = b) = P(\xi_0, \pi/2)$ (Figure 5). The deformed configuration of the ellipse is obtained by updating the semiaxes according to the displacement increments

$$a^i = a^{i-1} + \mathrm{d}u^i_{\max},\ b^i = b^{i-1} + \mathrm{d}u^i_{\min}, \tag{11}$$

where $\mathrm{d}u^i_{\max}$ and $\mathrm{d}u^i_{\min}$ are the incremental displacements obtained from the solution of the elliptical hole in the points $P_{\max}$ and $P_{\min}$, respectively. Finally, the minimum radius of curvature ϱ^i is computed from

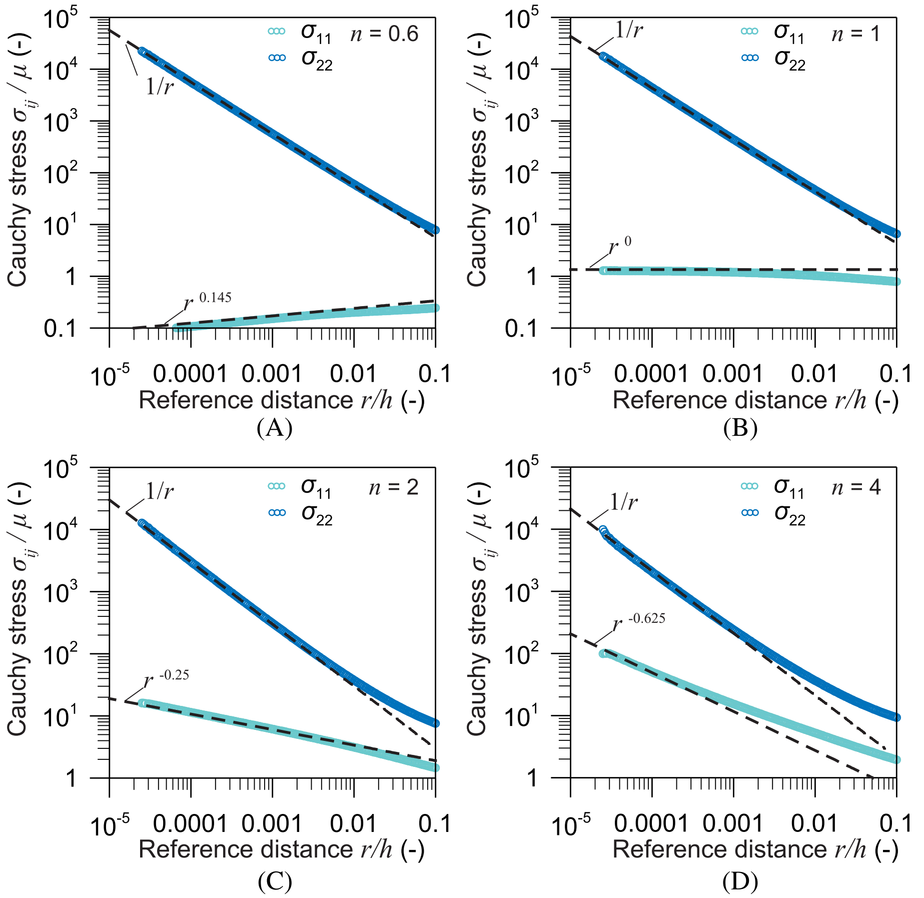

FIGURE 4 Crack-tip Cauchy stress components from FE analyses with respect to the normalized reference distance r/h, for $\vartheta = 0$ and $\lambda = 1.5$ (log scale). GNH model with (A) $n = 0.6$, (B) $n = 1$, (C) $n = 2$, (D) $n = 4$. Dashed lines correspond to the asymptotic trends predicted by the analytical solution (9). 2-col figure [Colour figure can be viewed at wileyonlinelibrary.com]

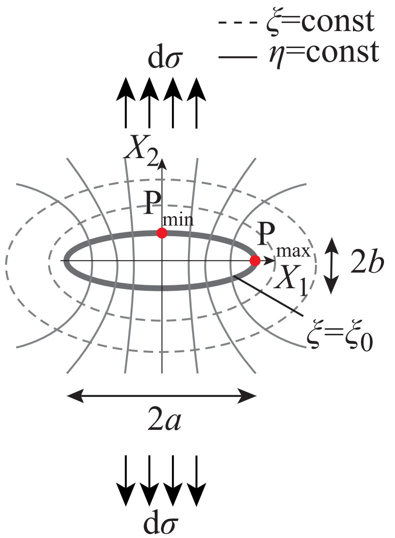

FIGURE 5 Elliptical deformed configuration in curvilinear elliptical coordinates. 1-col figure [Colour figure can be viewed at wileyonlinelibrary.com]

$$\varrho^i = \left(b^i\right)^2 / a^i. \tag{12}$$

To obtain a parameter that can be used to quantify the crack-tip blunting, we define a stress concentration factor $K_t = \sigma_{\max}/\sigma$, where $\sigma_{\max}$ is the stress at the minimum radius of curvature of the ellipse. For an elliptical notch in an infinite plate, the incremental value of the stress concentration factor is derived as[22]

$$K_t^i = \frac{\sigma_{\max}^i}{\sigma^i} = 1 + 2\sqrt{\frac{a^i}{\varrho^i}}. \tag{13}$$

The illustrative results according to the analytical model proposed are illustrated in Figure 6 (the relevant parameters adopted in the illustrative example are: $E = 3\mu = 1.12\text{MPa}, \nu = 0.42, G_c = 50\text{J/m}^2, a = 10\text{mm}$). We have also added a comparison with a model of elastic crack blunting proposed by Hui et al,[14] where the maximum notch root stress $\sigma_{\max}$ as a function of the applied stress σ is expressed as $\sigma_{\max} = 2\sigma/\left(\frac{\sigma}{E} + C\right)$, with $C = G_c/(\sigma_0 a), \sigma_0$ the strength of a cohesive crack and G_c the material fracture energy. The mitigation of the stress concentration factor at the blunted crack tip with increasing applied stretch λ is illustrated in Figure 6A, while Figure 6B shows the increase of the tip radius with λ. The LEFM solution of a center-cracked sample, described by

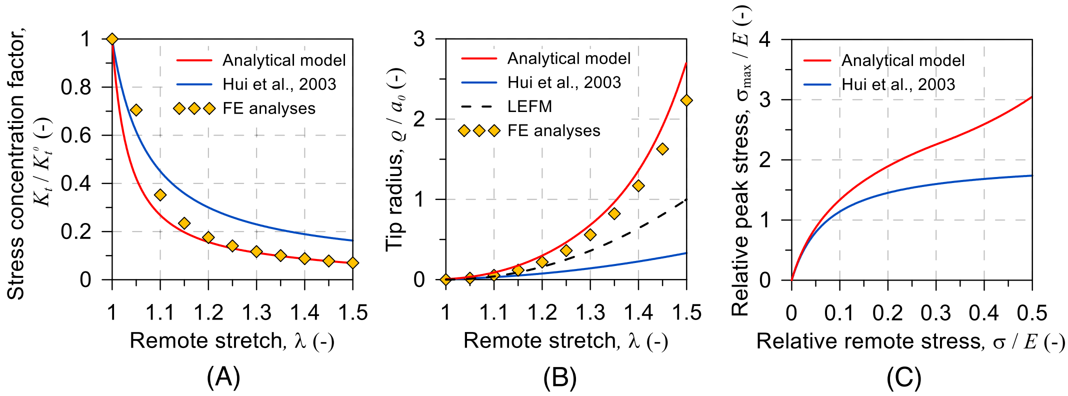

FIGURE 6 (A) Relative concentration factor as a function of the remote stretch. (B) Tip radius normalized with respect to the initial crack length as a function of the remote stretch. The dashed line corresponds the LEFM solution (14). (C) Relative peak stress at the crack tip versus relative remote stress. The blue curves are related to a model proposed by Hui et al.[14] 2-col figure [Colour figure can be viewed at wileyonlinelibrary.com]

$$\varrho = 4a(\lambda - 1)^2, \tag{14}$$

is also plotted. Excellent agreement is shown by the model proposed compared to FE analysis on a center-cracked sample with linear elastic material and geometric nonlinearity. Finally, Figure 6C describes the increase of the peak stress at the blunted crack tip as a function of the remote applied stress. Here, we observe that the model by Hui et al[14] exhibits an asymptotic trend, whereas the present model shows an inflection point corresponding to the inversion of the semiaxes of the ellipse.

3.2 | Experiments on silicone samples

We have performed tensile experiments on silicone rubber samples containing centered cracks of different lengths, which were stretched under displacement control with a constant nominal strain rate $\dot{\varepsilon} = 10^{-3}\mathrm{s}^{-1}$ up to complete failure. All the mechanical tests were performed using a universal testing machine Galdabini Quasar 2.5, equipped with a 3-kN load cell, while pictures are taken by means of a Basler acA5472-17uc USB 3.0 camera.

3.2.1 | Material characterization

The first set of experiments is performed on samples made of a commercial silicone rubber (Elite Double 32 by Zhermack Dental). First, tensile specimens are manufactured and tested at an average strain rate of $\dot{\varepsilon} = 10^{-3}\mathrm{s}^{-1}$ in order to characterize the mechanical parameters of the material. As shown in Figure 7A, the hyperelastic GNH strain-energy function in (3) can be fitted to the experimental uniaxial stress–strain curve taking $b = n = 1$, which corresponds to a neo-Hookean material model. Considering incompressibility, the initial Young's modulus is equal to $E = 3\mu = 1.22\,\mathrm{MPa}$. Further tests are conducted on pure-shear specimens, at an average strain rate of $\dot{\varepsilon} = 1 \cdot 10^{-3}\mathrm{s}^{-1}$, in order to obtain the fracture energy. In a pure-shear deformation, the fracture energy is independent of the crack length and is simply computed as $G_c = 2\Psi(\lambda_c)h$,[9] where $\Psi(\lambda_c)$ is the strain-energy per unit volume (3) computed at $\lambda = \lambda_c$, with λ_c the failure stretch of the pure-shear specimens ($G_c = 1.16\,\mathrm{N/mm}$, see Figure 7B). A second set of experiments deals with samples made of a different commercial silicone rubber (TSE3478T by Momentive), whose initial Young's modulus is taken to be equal to $E = 3\mu = 1.12\,\mathrm{MPa}$ ($G_c = 1.0\,\mathrm{N/mm}$, estimated).[25] Finally, a third set of experiments is related to a polydimethylsiloxane (PDMS) silicone (commercially named Sylgard 184), whose initial Young's modulus is here found to be equal to $E = 3\mu = 2.12\,\mathrm{MPa}$ ($G_c = 1.3\,\mathrm{N/mm}$, estimated[26]).

3.2.2 | Tearing of center-cracked samples

A summary of the tests on center-cracked samples is presented in Table 1, reporting an identification code, the geometry of the specimens and the failure stretch λ_c. A sketch of the experimental setup is shown in Figure 8A.

Results of the experiments are illustrated in Figure 8B–D. The experimentally obtained normalized crack tip radius ϱ/a is plotted in Figure 8B as a function of the stretch. A representative example of the experiments is illustrated in Figure 9 for a CC1 specimen. The analytical prediction obtained from the authors' model,

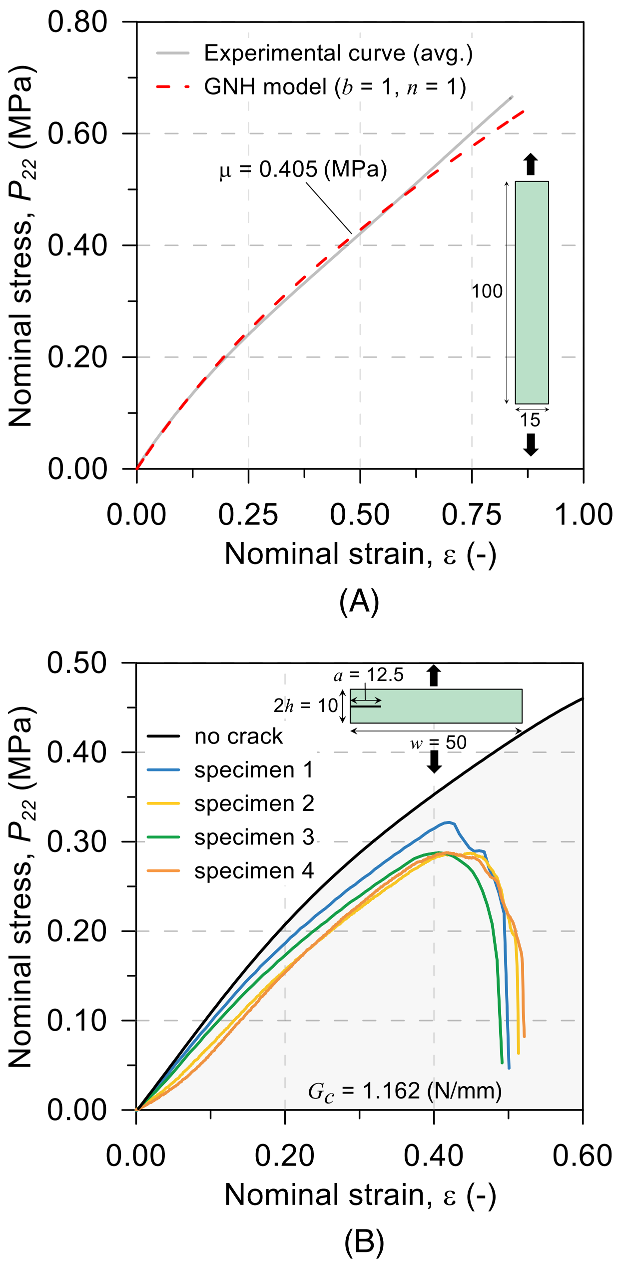

FIGURE 7 Mechanical characterization of the Elite Double 32 silicone. All the samples are tested at a nominal strain rate $\dot{\varepsilon} = 10^{-3}\text{s}^{-1}$. (A) Dimensions (mm) of the tensile specimens and model fitting of the experimentally obtained stress-stretch curve. (B) Dimensions (mm) of the pure-shear specimens and experimentally obtained stress-stretch curves. 1-col figure [Colour figure can be viewed at wileyonlinelibrary.com]

together with the LEFM solution (14) and the model proposed by Hui et al,[14] are added as comparison. It appears that the radius of curvature increases more rapidly in comparison to the LEFM prediction as the initial crack length gets larger.

Figure 8C plots the failure stretch λ_c as a function of the characteristic length a of the initial crack. According to LEFM, stretch at failure follows a decreasing power-law dependence on the crack length, provided by[21]

$$\lambda_c \sim 1 + \sqrt{\frac{G_c}{\pi E}}a^{-1/2}, \tag{15}$$

where it was assumed that the remote stress is $\sigma \sim \sqrt{GE/\pi a}$ and considering the failure criterion $G = G_c$. In Figure 8C, the best-fit curves with a power-law dependence with exponent -0.5 are shown along with the LEFM solution (15). The overall trend of experimental results seems to be well described by the power law dependence of LEFM.

Finally, the experimental results are elaborated in order to quantify the effect of crack blunting in terms of failure. Let us define the quantity $K_t(\lambda_c - 1)$, where λ_c is the ultimate stretch derived from the experiments (Table 1) and K_t is the stress concentration factor corresponding to λ_c, computed from the analytical model (13). The quantity $K_t(\lambda_c - 1)$ represents the normalized true stress at the notch root at incipient failure and can be considered as an intrinsic material property, independent of the presence of the flaw. The results are summarized in Figure 8D.

4 | DISCUSSION

Within the framework of continuum mechanics, the fracture process is connected to a length parameter, which originates from the competition between surface energy for crack propagation and bulk deformation energy.[2] This quantity, known in the literature as elasto-adhesive length, represents the minimum length of a crack below which failure becomes flaw-insensitive.[3] This is a central concept in fracture mechanics and becomes particularly relevant with respect to soft materials, since it can be related to the radius of a blunted crack-tip.[2]

In order to understand how crack blunting affects fracture of soft materials, it is mandatory to account for the nonlinearity associated with large deformation of the crack. This aspect requires to analyze the crack-tip zone according to the full nonlinear theory of elasticity. The results reviewed in Section 2 provide a drastically different picture with respect to linear elastic fracture mechanics (LEFM). In particular, the crack-tip stress field is dominated by a single component and is deeply affected by the degree of strain hardening. As a consequence, the crack-tip field might be characterized by a nearly hydrostatic state (where singularities of the stress components have similar magnitudes) or by a uniaxial state (where the opening stress has a stronger singularity). Even more remarkable is the effect in terms of deformed crack

TABLE 1 Geometric characteristics of center-cracked silicone specimens with different crack lengths (w = specimen half width, h = specimen half height, t = specimen thickness, a = crack semi-length, $h/w \approx 2$ for all specimens)

ID	w(mm)	a(mm)	t(mm)	a/w	λ_c
Elite Double 32					
CC1	24.9	2	2.62	0.080	1.40
CC2	24.8	4	2.39	0.162	1.25
CC3	24.7	8	2.56	0.324	1.20
CC4	24.8	10	2.56	0.403	1.16
CC5	24.8	14	2.95	0.565	1.13
CC6	24.8	17	2.31	0.684	1.11
TSE3478T					
CC7	56	10	2.75	0.179	1.75
CC8	56	15	3	0.268	1.61
CC9	56	20	2.75	0.357	1.55
CC10	56	25	2.85	0.446	1.32
Sylgard 184					
CC11	28.4	7	2.54	0.247	1.09
CC12	27.9	12	3.07	0.431	1.08
CC13	28.2	18	2.57	0.639	1.06

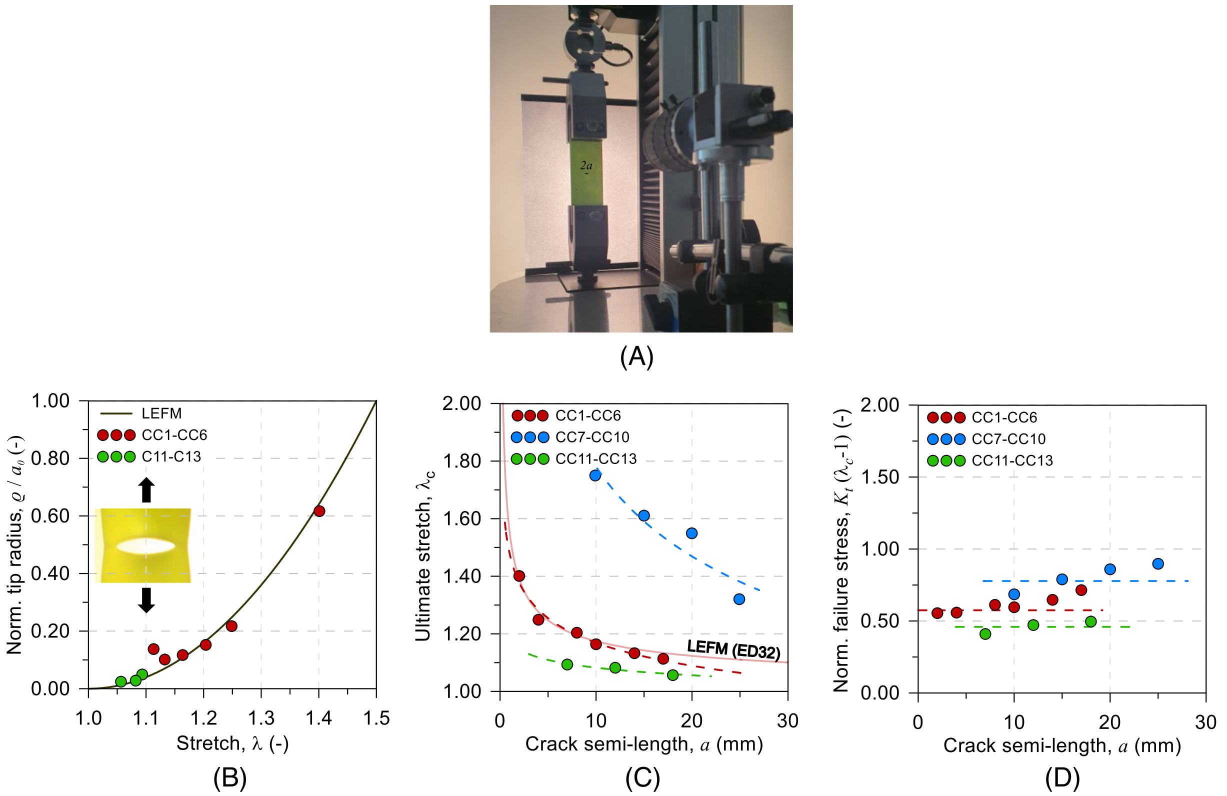

FIGURE 8 (A) Experimental setup. (B) Crack tip radius against remote stretch at failure (experimental results for CC1–CC6 and CC11–CC13 specimens). (C) Stretch at failure λ_c as a function of the initial crack semi-length a_0. The continuous light red line corresponds to the prediction of the LEFM solution (15) while the dashed lines represent the best-fit curves with a power law dependence with exponent −0.5. (D) Normalized true stress at incipient failure versus initial crack semilength a_0. The dashed lines represent the average values of $K_t(\lambda_c - 1)$. 2-col figure [Colour figure can be viewed at wileyonlinelibrary.com]

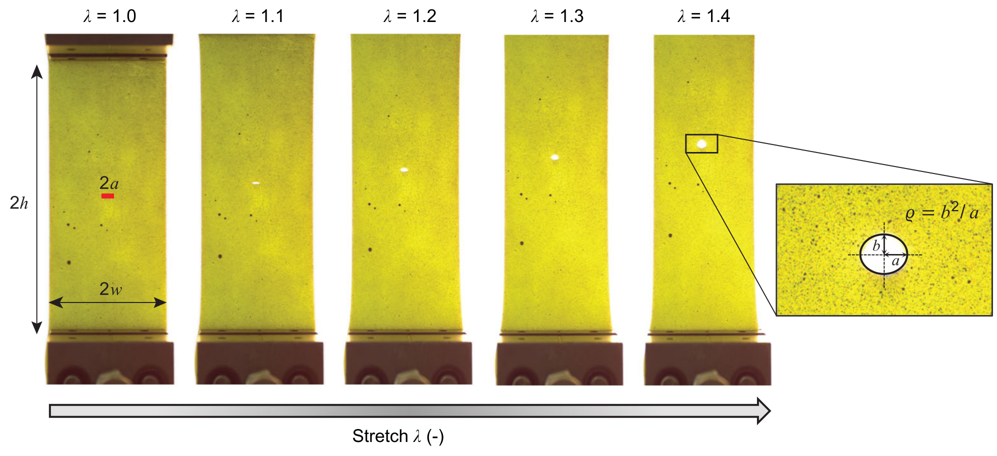

FIGURE 9 Initial and increasingly deformed configurations at different applied stretches of a CC1 specimen. The inset in the last frame shows the deformed elliptic profile of the crack. 2-col figure [Colour figure can be viewed at wileyonlinelibrary.com]

profiles, with strain hardening leading to reduced blunting and high stress gradients concentrated in a small region surrounding the crack-tip.

In terms of failure, blunting has major effects, which can be appreciated with the model proposed. Although derived for linear elasticity, the model seems to behave accurately for large deformations when compared with finite element simulations (Figure 6). Besides providing a description of the evolution of the blunted crack-tip with increasing deformation, the model can be used to infer some conclusions on the failure condition in soft materials. A normalized stress at the notch root provides an adequate parameter for evaluating the failure of cracked samples subjected to large deformation. Differently from the fracture-mechanics related quantities, which show a dependence on the size of the crack, the parameter proposed is a mechanical property of the material. Furthermore, being related to the tip radius of the blunted crack, it directly relates crack-tip blunting with the concept of a flaw-insensitive failure. As a matter of fact, the model gives a relation between the peak stress at the crack tip or the tip radius and the remote stretch: A critical condition of fracture can then be identified by comparing these values with a cohesive stress or with a material-related critical crack tip displacement.

In this work, we have attempted to validate the model through experiments on center-cracked silicone samples. The crack-tip radius observed seems to be quite different from the predictions of LEFM (Figure 8B). However, this is not directly reflected in terms of the failure stretch, which seems to follow the size dependent predictions of LEFM (Figure 8C). We hypothesize that the failure criterion based on the local stress, and hence the concept of a flaw-insensitive failure, might become more appropriate in tougher soft materials, where severe crack blunting is developed before failure and the elasto-adhesive length is larger.

5 | CONCLUSIONS

The present paper is devoted to the study of crack-tip stress fields in soft materials. FE analyses were carried out on pure-shear geometries considering incompressible hyperelastic models with strain hardening. The analytical asymptotic solutions are presented together with the results obtained from FE analyses. The elastic crack-tip blunting under loading is quantified by a local radius of curvature at the crack tip, which is found to strongly depend on the degree of strain hardening. A geometric nonlinear analytical model, introduced to describe the progressive blunting of the crack tip in a linear elastic material under remote mode I loading, is compared to experimental results on center-cracked silicone specimens. The model provides a condition, alternative to LEFM, to identify the critical condition of crack propagation in soft materials.

ACKNOWLEDGMENTS

The authors would like to thank the support from EU Horizon 2020 Research and Innovation Programme (H2020-WIDESPREAD-2018, SIRAMM) under Grant Agreement No. 857124. Open Access Funding provided by Universita degli Studi di Parma within the CRUI-CARE Agreement.

ORCID

Andrea Spagnoli https://orcid.org/0000-0002-0592-7003

REFERENCES

1. Doi M. *Soft Matter Physics*. OUP Oxford; 2013.
2. Creton C, Ciccotti M. Fracture and adhesion of soft materials: a review. *Reports on Progress in Physics*. 2016;79:046601.
3. Chen C, Wang Z, Suo Z. Flaw sensitivity of highly stretchable materials. *Extreme Mechanics Letters*. 2017;10:50-57.
4. Holzapfel GA. Similarities between soft biological tissues and rubberlike materials. *Constitutive Models for Rubber IV*. 2005: 1-11.

5. Terzano M, Spagnoli A, Ståhle P. A fracture mechanics model to study indentation cutting. *Fatigue & Fracture of Engineering Materials and Structures*. 2018;41:821-830.
6. Terzano M, Dini D, Rodriguez y Baena F, Spagnoli A, Oldfield M. An adaptive finite element model for steerable needles. *Biomechanics and Modeling in Mechanobiology*. 2020;19(5):1809-1825.
7. Shull KR. Fracture and adhesion of elastomers and gels: large strains at small length scales. *Journal of Polymer Science Part B: Polymer Physics*. 2006;44:3436-3439.
8. Knowles JK. The finite anti-plane shear field near the tip of a crack for a class of incompressible elastic solids. *International Journal of Fracture*. 1977;13:611-639.
9. Rivlin RS, Thomas AG. Rupture of rubber. I. Characteristic energy for tearing. *Journal of Polymer Science*. 1953;10:291-318.
10. Thomas AG. Rupture of rubber. II. The strain concentration at an incision. *Journal of Polymer Science*. 1955;18:177-188.
11. Long R, Hui C-Y. Crack tip fields in soft elastic solids subjected to large quasi-static deformation—a review. *Extreme Mechanics Letters*. 2015;4:131-155.
12. Spagnoli A, Brighenti R, Cosma MP, Terzano M. Chapter two - fracture in soft elastic materials: continuum description, molecular aspects and applications. *Advances in Applied Mechanics*. 2022;55:255-307.
13. Yang W, Sherman VR, Gludovatz B, et al. On the tear resistance of skin. *Nature Communications*. 2015;6:6649.
14. Hui C-Y, Jagota A, Bennison SJ, Londono JD. Crack blunting and the strength of soft elastic solids. *Proceedings of the Royal Society A: Mathematical, Physical and Engineering Sciences*. 2003;459:1489-1516.
15. Zhou Y, Hu J, Zhao P, Zhang W, Suo Z, Lu T. Flaw-sensitivity of a tough hydrogel under monotonic and cyclic loads. *Journal of the Mechanics and Physics of Solids*. 2021;153:104483.
16. Holzapfel GA. *Nonlinear Solid Mechanics: A Continuum Approach for Engineering Science*. Wiley; 2000.
17. Horgan CO, Smayda MG. The trousers test for tearing of soft biomaterials. *International Journal of Solids and Structures*. 2012;49:161-169.
18. Geubelle PH, Knauss WG. Finite strains at the tip of a crack in a sheet of hyperelastic material: I. Homogeneous case. *Journal of Elasticity*. 1994;35:61-98.
19. Long R, Krishnan VR, Hui C-Y. Finite strain analysis of crack tip fields in incompressible hyperelastic solids loaded in plane stress. *Journal of the Mechanics and Physics of Solids*. 2011;59:672-695.
20. Kuna M. *Finite Elements in Fracture Mechanics: Theory - Numerics - Applications*: Springer Netherlands; 2013.
21. Anderson TL. *Fracture Mechanics: Fundamentals and Applications*. Third. CRC Press/Taylor and Francis; 2005. Nice and simple books on Fracture Mechanics.
22. Inglis CE. Stresses in a plate due to the presence of cracks and sharp corners. *Transactions of the Institution of Naval Architects*. 1913;55:219-230.
23. Timoshenko S, Goodier JN. *Theory of Elasticity*. McGraw-Hill; 1951.
24. Gao X-L. A general solution of an infinite elastic plate with an elliptic hole under biaxial loading. *International Journal of Pressure Vessels and Piping*. 1996;67:95-104.
25. Spagnoli A, Terzano M, Brighenti R, Artoni F, Carpinteri A. How soft polymers cope with cracks and notches. *Applied Sciences*. 2019;9:1086.
26. Moučka R, Sedlačík M, Osička J, Pata V. Mechanical properties of bulk Sylgard 184 and its extension with silicone oil. *Scientific Reports*. 2021;11(1):1-9.

How to cite this article: Spagnoli A, Brighenti R, Montanari M, Terzano M. Crack-tip blunting and its implications on fracture of soft materials. *Fatigue Fract Eng Mater Struct*. 2023;1-11. doi:10.1111/ffe.13951